Journal of Coordination Chemistry

ISSN: 0095-8972 (Print) 1029-0389 (Online) Journal homepage: http://www.tandfonline.com/loi/gcoo20

Synthesis, crystal structure, and interaction with DNA and BSA of a chromium(III) complex with naph-gly Schiff base and 1,10-phenanthroline

Hongyan Liu, Qiong Guo, Jianfang Dong, Qiang Wei, Han Zhang, Xubo Sun, Cuicui Liu & Lianzhi Li

To cite this article: Hongyan Liu, Qiong Guo, Jianfang Dong, Qiang Wei, Han Zhang, Xubo Sun, Cuicui Liu & Lianzhi Li (2015) Synthesis, crystal structure, and interaction with DNA and BSA of a chromium(III) complex with naph-gly Schiff base and 1,10-phenanthroline, Journal of Coordination Chemistry, 68:6, 1040-1053, DOI: 10.1080/00958972.2015.1007963

To link to this article: http://dx.doi.org/10.1080/00958972.2015.1007963

Accepted author version posted online: 19 Jan 2015.
Published online: 11 Feb 2015.

Journal of Coordination Chemistry, 2015
Vol. 68, No. 6, 1040–1053, http://dx.doi.org/10.1080/00958972.2015.1007963

Synthesis, crystal structure, and interaction with DNA and BSA of a chromium(III) complex with naph-gly Schiff base and 1,10-phenanthroline

HONGYAN LIU†, QIONG GUO†, JIANFANG DONG†‡, QIANG WEI†, HAN ZHANG†, XUBO SUN†, CUICUI LIU† and LIANZHI LI*†

†School of Chemistry and Chemical Engineering, Liaocheng University, Liaocheng, PR China
‡Department of Material Science, Shandong Polytechnic Technician College, Liaocheng, PR China

(*Received 5 May 2014; accepted 30 December 2014*)

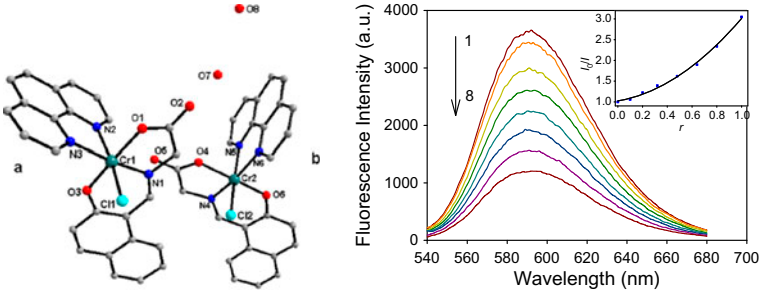

A new chromium(III) complex, [CrCl(naph-gly)phen]·H_2O, with a Schiff base derived from 2-hydroxy-1-naphthaldehyde and glycine and with 1,10-phenanthroline as a co-ligand has been synthesized and characterized by IR and single-crystal X-ray diffraction. The interactions of the complex with DNA and BSA have been investigated by UV absorption, fluorescence, and CD spectra.

A new chromium(III) complex, [CrCl(naph-gly)phen]·H_2O (naph-gly = Schiff base derived from 2-hydroxy-1-naphthaldehyde and glycine, phen = 1,10-phenanthroline), has been synthesized and characterized by elemental analysis, electrospray ionization mass spectroscopy, FT-IR, and X-ray single-crystal diffraction. The chromium(III) complex belongs to the trigonal crystal system, P3(1) space group with crystallographic data: $a = b = 1.97017(16)$ nm, $c = 1.02991(7)$ nm, $\alpha = \beta = 90°$, $\gamma = 120°$, $V = 3.4621(5)$ nm^3, $D_c = 1.476$ g·cm^{-3}, $Z = 6$, $F(0\ 0\ 0) = 1578$, $R_1 = 0.0508$, $wR_2 = 0.0907$. There are two independent molecules in the crystallographic asymmetric unit of the chromium(III) complex. Each Cr^{III} is six-coordinate to form an octahedral geometry. In the crystal, a 3-D structure is formed through intermolecular hydrogen bonds. The calf thymus DNA (CT-DNA)- and bovine serum albumin (BSA)-binding properties of the complex have been studied by UV absorption, fluorescence, and circular dichroism (CD) spectroscopy. Results indicate that the chromium(III) complex binds to CT-DNA in an intercalative mode, and it can bind to BSA and cause conformational changes of BSA.

Keywords: Chromium(III) complex; Glycine; Schiff base; DNA; BSA

*Corresponding author. Email: lilianzhi@lcu.edu.cn

1. Introduction

Schiff bases have played an important role in the development of coordination chemistry because they can form stable complexes with the overwhelming majority of transition metals. Furthermore, amino acid Schiff base complexes of transition metal have been attracting attention because of their importance in different fields, such as medicinal chemistry [1–4]. Chromium was proposed to be an essential trace element over 50 years ago and has been accepted as an essential element for 30 years. However, recent research has shown that chromium is probably not an essential element, but it has pharmacological effects at high doses, affecting carbohydrate and lipid metabolism in rodent models of insulin sensitivity [5]. The mechanism of the pharmacological effects of chromium(III) is still an area requiring continued research.

Chromium(III) chloride can bring about DNA crosslinking. Ligands play a vital role in the biological activity of trivalent chromium. Chromium(III) picolinate causes chromosomal damage [6]; chromium(III) Schiff base complexes exhibit nuclease activity [7]. Several studies of the binding of Cr(III) Schiff bases to both DNA and albumin have been studied by Nair's group. Chromium(III) complexes, such as $[Cr(DPPZ)_2Cl_2]$, a planar bidentate ligand with an extended aromatic system, and a Schiff base complex, $[Cr(naphen)(H_2O)_2]^+$, bind strongly to CT-DNA in an intercalative mode [8, 9]. The chromium(III) complex also brought about protein crosslink formation [10]. However, few Cr(III) amino acid Schiff base complexes have been synthesized [11]. Understanding of the interactions between amino acid Schiff base Cr(III) complexes and DNA as well as bovine serum albumin (BSA) are still lacking. In our previous work, we have synthesized and structurally characterized several amino acid Schiff base complexes [12–16]. To continue our research in this project, herein, a new Cr(III) complex containing a Schiff base ligand derived from L-glycine and 2-hydroxy-1-naphthaldehyde with 1,10-phenanthroline as a co-ligand has been synthesized and characterized. Further, the DNA-binding and BSA-binding properties of the complex have been studied by UV, fluorescence, and circular dichroism (CD) spectroscopy. Results will be helpful to understand the binding of such Cr(III) complexes to DNA and BSA, and useful for exploring new anticancer agents and antidiabetic agents, biomolecular modification, and detection.

2. Experimental

2.1. *Materials*

2-Hydroxy-1-naphthaldehyde was purchased from Fluka and glycine was obtained from Beijing Jingke Company. calf thymus DNA (CT-DNA) and BSA were purchased from the Sino-American Biotechnology Company (China). Ethidium bromide (EB) was purchased from Sigma (USA). All other chemicals were AR grade and used without purification. Solutions of CT-DNA in 10 mM L^{-1} Tris–HCl/10 mM L^{-1} NaCl (pH 7.1) buffer gave a ratio of UV absorbance at 260 and 280 nm (A_{260}/A_{280}) of 1.8–1.9, indicating that the DNA was sufficiently free of protein [17]. The CT-DNA concentration per nucleotide was determined by absorption spectroscopy using the molar absorption coefficient (6600 $(M\ L^{-1})^{-1}\ cm^{-1}$) at 260 nm [18]. The BSA stock solution (20 mM L^{-1} based on its molecular mass of 66,000 Da) in 10 mM L^{-1} Tris–HCl/10 mM L^{-1} NaCl (pH 7.1) buffer was stored in the

dark prior to use. The solutions of EB and the chromium(III) complex were prepared by 10 mM L^{-1} Tris–HCl/10 mM L^{-1} NaCl buffer and their concentrations were calculated by the ratio of mass to their molecular weight.

2.2. *Synthesis of CrCl(naph-gly)phen*

Glycine (0.15 g, 2.0 mM) and potassium hydroxide (0.11 g, 2.0 mM) were dissolved in absolute methanol (15 mL) and added successively to a methanol solution (5.0 mL) of 2-hydroxy-1-naphthaldehyde (0.34 g, 2.0 mM). The mixture was then stirred at 55 °C for 2 h. Subsequently, a methanol solution (3.0 mL) of chromium chloride hexahydrate (0.53 g, 2.0 mM) was added dropwise and stirred for 3.0 h. A methanol solution (5.0 mL) of 1,10-phenanthroline (0.40 g, 2.0 mM) was added dropwise and stirred for another 5.0 h. The resultant solution was filtered and held at room temperature for 3 days, whereupon red blocky single crystals suitable for X-ray diffraction analysis were obtained. Yield: 63%. Anal. Calcd for $C_{25}H_{19}ClCrN_3O_4$ (%): C, 58.55; H, 3.73; N, 8.19. Found (%): C, 58.51; H, 3.75; N, 8.15. IR (KBr, ν/cm^{-1}; s, strong absorption; m, middle absorption; w, weak absorption) cm^{-1}: 3418 (m), 1617 (s), 1601 (s), 1575 (m), 1539 (m), 1520 (m), 1457 (w), 1424 (m), 1380 (m), 1340 (m), 1306 (w), 1251 (w), 1188 (w), 1144 (w), 1107 (w), 967 (w), 875 (w), 850 (w), 741 (w), 722 (m), 654 (w), 578 (w), 529 (w), 499 (w), 433 (w).

2.3. *Physical measurements*

Elemental analyses for C, H, and N were performed on a Perkin–Elmer 2400 II analyzer. Infrared spectrum was obtained with a KBr pellet on a Nicolet 5700 FT-IR from 4000 to 400 cm^{-1}. Electrospray ionization mass spectroscopic (ESI-MS) analyses are performed with a Thermo Finnigan LCQ-DECA mass spectrometer, and the mass spectra are obtained in the positive mode. UV–visible absorption spectra were recorded on a Hewlett-Packard HP-8453A Diode Array spectrophotometer. Fluorescence spectra were recorded on an LS55 spectrofluorometer. CD spectral measurements were measured on a Jasco J-810 spectropolarimeter.

2.4. *X-ray crystallographic analysis*

A single crystal of the complex with dimensions 0.28 mm × 0.14 mm × 0.12 mm was mounted in a glass capillary and data were collected on a Bruker Smart-1000 CCD diffractometer. Intensity data were collected with graphite monochromated Mo Kα radiation ($\lambda = 0.071073$ nm) at 298(2) K in the range of $2.31° < \theta < 25.01°$ with the ω-scan technique. A semi-empirical absorption correction was applied using SADABS [19] to all the data. The structure was solved by direct methods using SHELXLS-97 and refined against F^2 by full-matrix least squares using SHELXL-97 [20, 21]. The hydrogens of water molecules were found in difference Fourier maps and the O–H distances standardized to 0.85 Å. The organic hydrogens were generated geometrically and allowed to refine using a riding model. A summary of pertinent crystal data, experimental details, and refinement results are shown in table 1.

Table 1. Crystallographic and structure refinement data for the complex.

Empirical formula	$C_{25}H_{19}ClCrN_3O_4$
Formula weight	512.88
Temperature (K)	298(2)
Wavelength (Å)	0.71073
Crystal system, space group	Trigonal, P3(1)
Unit cell dimensions	
$a = b$ (Å)	19.7017(16)
c (Å)	10.2991(7)
$\alpha = \beta$ (°)	90
γ (°)	120
Volume (Å^3)	3462.1(5)
Z, Calculated density (Mg m^{-3})	6, 1.476
Absorption coefficient (mm^{-1})	0.649
F(0 0 0)	1578
Crystal size (mm)	0.28 × 0.14 × 0.12
θ Range for data collection (°)	2.31–25.01
Completeness to theta = 25.01 (%)	100.0
Limiting indices	−22, 23; −21, 23; −6, 12
Reflections collected/unique	17,786/6208
R(int)	0.0821
Data/restraints/parameters	6208/2090/613
Goodness-of-fit on F^2	0.985
Final R indices [$I > 2\sigma(I)$]	$R_1 = 0.0508$, $wR_2 = 0.0831$
R indices (all data)	$R_1 = 0.0916$, $wR_2 = 0.0907$
Absolute structure parameter	−0.02(2)
Largest difference in peak and hole (e Å^{-3})	0.489 and −0.366

2.5. *DNA-binding experiments*

All the DNA-binding experiments were carried out in 10 mM L^{-1} Tris–HCl/10 mM L^{-1} NaCl, pH 7.1 buffer solution. The UV–visible absorption spectra of complex binding to CT-DNA were performed by increasing amounts of DNA to complex in buffer solution. The mixed solutions were incubated for 2 h before the absorption spectra were recorded.

The fluorescence spectra were carried out by adding the complex to EB-bound CT-DNA solutions after they had been incubated for 2 h at room temperature. The emission spectra were recorded from 540 to 680 nm at an excitation wavelength of 258 nm with slit width of 5 nm for both excitation and emission.

The CD spectra of DNA incubated with the complex were obtained using 1 cm path length quartz cells at wavelengths between 220 and 320 nm. The changes in CD spectra were monitored against the corresponding blanks. Each CD spectrum was reported as the average of three scans using a scan speed of 100 nm min^{-1} and a 1 s response time.

2.6. *BSA-binding experiments*

All the BSA-binding experiments were carried out in 10 mM L^{-1} Tris–HCl/10 mM L^{-1} NaCl, pH 7.1 buffer solutions. The electronic absorption spectra of BSA (5×10^{-7} M L^{-1}) titrated by the complex were recorded from 200 to 300 nm using a 1 cm quartz cell. Buffer or solutions of the corresponding concentrations for complex were placed in the reference.

The fluorescence emission spectra of BSA with increase in the concentrations of the complex were recorded at 298 K from 300 to 460 nm under an excitation wavelength of

295 nm, with a scan rate of 200 nm min^{-1}. The slit widths were set to 7 nm for both excitation and emission.

CD spectra of BSA in the absence and presence of the complex were recorded from 200 to 250 nm at room temperature with a quartz cell of 0.1 cm path length under constant nitrogen flush. Each spectrum was the average of three accumulations at a scan rate of 100 nm min^{-1} and a response time of 1 s. The corresponding absorbance contributions of buffer and the complex solutions were recorded and subtracted with the same instrumental parameters.

3. Results and discussion

3.1. *IR spectra and ESI-MS*

In IR spectra of the complex, the sharp absorption at 1638 cm^{-1} can be assigned to the imine group (C=N) stretching frequency of the coordinated Schiff base ligands in the complex. The absorptions at 1541 and 1340 cm^{-1} for the complex are attributed to asymmetric and symmetric stretching vibration of CO_2^-, respectively. The frequency separation ($\Delta\nu$) is greater than 200 cm^{-1}, which reflects the coordination modes of carboxyl group, suggesting a unidentate bonding nature for the carboxylate ligation [22]. The ν_{C-O} (phenolic) stretching frequency was observed at 1251 cm^{-1} in the complex, indicating bonding through phenolic oxygen [23]. The complex also showed weak intensity bands at 529, 499, and 433 cm^{-1}, which could be attributed to Cr–N, Cr–O, and Cr–Cl absorptions, respectively.

The positive ion ESI-MS of the chromium(III) complex [CrCl(naph-gly)phen]·H_2O showed three distinct peaks because of the formation of different ions, m/z = 935.03 {[Cr(naph-gly)phen](OH)[Cr(naph-gly)phen]}$^+$, 498.64 {[Cr(OH)(naph-gly)phen] + Na}$^+$, and 264.56 {[Cr(Cl)(naph-gly)phen] + $2NH_4$}$^{2+}$. In addition, there are some smaller peaks because of the formation of other ions. The result showed that the coordinated Cl^- is replaced by OH^-, and in addition to monomeric ion, there exist dimeric ions in solution.

3.2. *Description of crystal structure*

The crystal structure of the complex has been determined by single-crystal X-ray diffraction. As shown in figure 1, there are two independent molecules in an asymmetric unit. Each Cr(III) is six-coordinate to form an octahedral geometry by one terminal chloride, two oxygens, and one nitrogen from the amino acid Schiff base, and two nitrogens of 1,10-phenanthroline. The selected bond lengths and angles around Cr(III) are given in table 2. In molecule **a**, Cl1 and N2 lie in axial positions of the octahedral geometry with the *trans* angle of 170.28(17)°; O1, O3, N1, and N3 are in the equatorial plane of the octahedron. The Cr1 ion lies 0.0929(25) Å above the equatorial plane towards N2 with Cr1–N2 = 2.069(5) Å and Cr1–Cl1 = 2.3024(18) Å. The phenanthroline coordinates to Cr1 almost vertical to the equatorial plane with the dihedral angle 89.39(12)°. In molecule **b**, Cl2 and N5 occupy the axial positions of the octahedral geometry with the *trans* angle of 171.71(18)°. The equatorial plane of the octahedron is formed by O4, O6, N4, and N6 atoms. Cr2 is situated 0.1215(26) Å above the equatorial plane toward N5 with

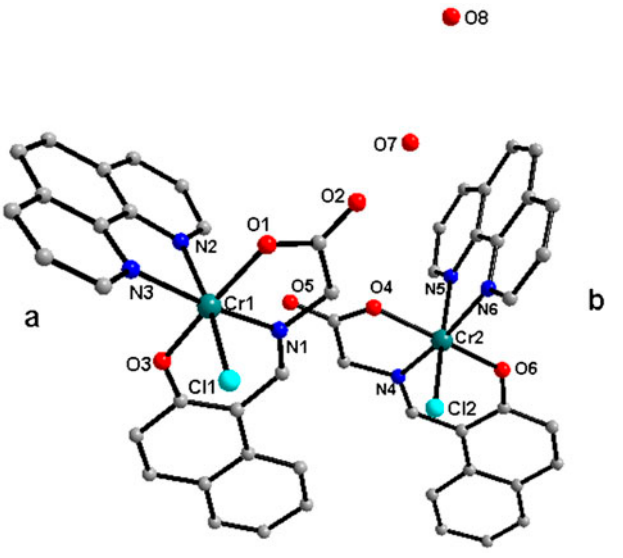

Figure 1. ORTEP view of the molecular structure with part atom-labeling scheme of the chromium(III) complex. (a) molecule a; (b) molecule b. O7 and O8 present two water molecules. The hydrogen atoms are omitted for clarity.

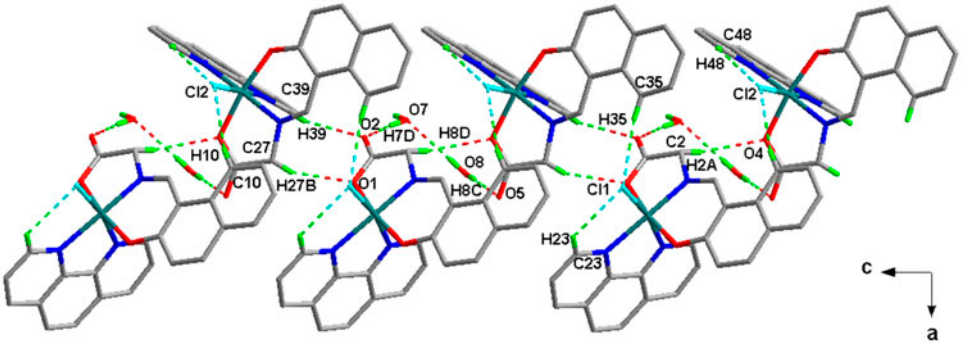

Figure 2a. 1-D chain structure formed by the dimers.

Cr2–N5 = 2.095(6) Å and Cr2–Cl2 = 2.281(2) Å. The dihedral angle formed by the equatorial plane and the phenanthroline ligand is 86.97(14)°.

There are some important intermolecular and intramolecular hydrogen bonds in the crystal. The related parameters and symmetry codes are listed in table 3. As shown in figure 2 (a), one molecule **a** and one molecule **b** formed a dimer via intramolecular hydrogen bonds C27–H27B···O1, C39–H39···O2, and C35–H35···Cl1. The dimers further connected through intermolecular hydrogen bonds C10–H10···Cl2c and C2–H2A···O4^{c} and hydrogen bonds involve water molecules O7–H7D···O2, O8–H8C···O5, and O8–H8D···O7^{b} to form a 1-D chain structure along the *c* axis. These 1-D chains are arranged parallel to each other and interacted through the hydrogen bonds C24–H24···O6^{e}, C50–H50···O5^{f}, and

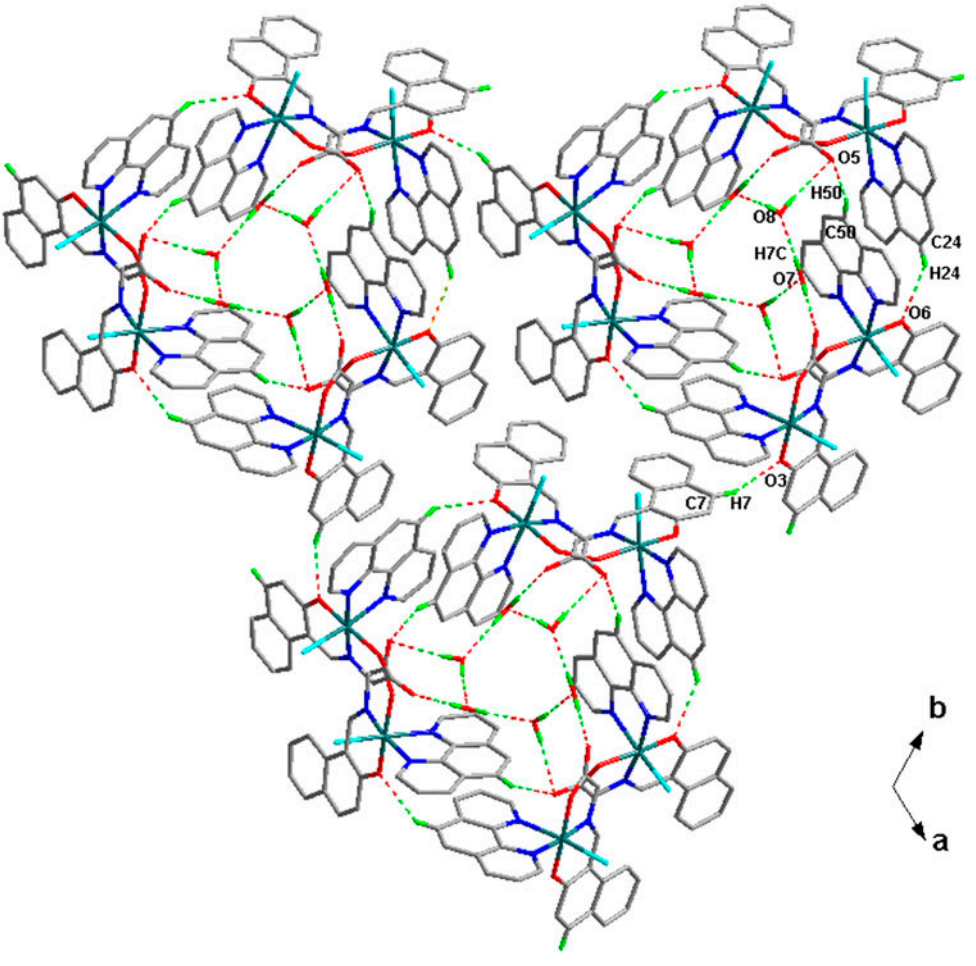

Figure 2b. 2-D structure formed by intermolecular hydrogen bonds.

O7–H7C···O8[a] to form a hexagonal prism structure [figure 2(b)]. Finally, a 3-D structure is formed by an intermolecular hydrogen bond C7–H7···O3d.

3.3. *DNA-binding studies*

3.3.1. UV spectroscopy. UV–visible absorption spectra are a useful method to investigate the interaction of complexes with DNA. Monitoring the changes in absorption spectrum of the metal complex upon addition of increasing amounts of DNA is widely used for determining overall binding constants. A complex binding to DNA through intercalation usually results in hypochromism and bathochromism involving strong stacking interaction between an aromatic chromophore and the base pairs of DNA [24]. The extent of hypochromism is consistent with strength of intercalative binding interaction [25, 26]. As shown in figure 3, there are two absorption peaks at 225 and 271 nm for the complex, which can be attributed

Table 2. Selected bond lengths (Å) and angles (°) for the complex.

Cr1–O3	1.918(4)	Cr1–O1	1.960(4)
Cr1–N1	1.979(5)	Cr1–N3	2.113(5)
Cr1–N2	2.069(5)	Cr1–Cl1	2.3024(18)
Cr2–O6	1.913(4)	Cr2–O4	1.966(4)
Cr2–N4	1.974(5)	Cr2–N6	2.106(6)
Cr2–N5	2.095(6)	Cr2–Cl2	2.281(2)
O3–Cr1–N1	89.66(18)	O3–Cr1–O1	169.89(18)
N1–Cr1–O1	82.43(19)	O3–Cr1–N2	87.96(18)
N1–Cr1–N2	97.1(2)	O1–Cr1–N2	86.78(18)
O3–Cr1–N3	94.01(18)	N1–Cr1–N3	174.3(2)
O1–Cr1–N3	93.41(18)	N2–Cr1–N3	78.6(2)
O3–Cr1–Cl1	92.23(13)	N1–Cr1–Cl1	92.59(14)
O1–Cr1–Cl1	94.41(12)	N2–Cr1–Cl1	170.28(17)
N3–Cr1–Cl1	91.65(16)	O6–Cr2–O4	170.41(19)
O6–Cr2–N4	90.2(2)	O4–Cr2–N4	82.70(19)
O6–Cr2–N6	93.0(2)	O4–Cr2–N6	93.3(2)
N4–Cr2–N6	172.0(2)	O6–Cr2–N5	88.87(19)
O4–Cr2–N5	78.5(2)	N4–Cr2–N5	94.2(2)
N6–Cr2–N5	174.7(2)	O6–Cr2–Cl2	94.01(14)
O4–Cr2–Cl2	92.85(13)	N4–Cr2–Cl2	93.54(14)
N6–Cr2–Cl2	93.56(19)	N5–Cr2–Cl2	171.71(18)

Table 3. Hydrogen bond lengths (Å) and angles (°) for the complex.

D–H···A	d(D–H)/Å	d(H···A)/Å	d(D···A)/Å	∠(DHA)/°
O7–H7D···O2	0.85	2.00	2.838(10)	169.6
O8–H8C···O5	0.85	2.52	3.366(10)	172.7
C23–H23···Cl1	0.93	2.70	3.269(7)	120.4
C48–H48···Cl2	0.93	2.71	3.281(8)	120.3
C27–H27B···O1	0.97	2.40	3.205(8)	140.1
C35–H35···Cl1	0.93	2.63	3.552(7)	169.2
C39–H39···O2	0.93	2.44	3.262(9)	147.4
O7–H7C···O8[a]	0.85	2.18	3.023(15)	169.2
O8–H8D···O7[b]	0.85	2.24	3.083(15)	173.4
C2–H2A···O4[c]	0.97	2.53	3.314(8)	138.1
C10–H10···Cl2[c]	0.93	2.77	3.690(7)	168.4
C7–H7···O3[d]	0.93	2.39	3.250(7)	154.5
C24–H24···O6[e]	0.93	2.57	3.374(8)	145.1
C50–H50···O5[f]	0.93	2.42	3.310(10)	159.8

Notes: Symmetry codes: (a) $-y+1,\ x-y,\ z-2/3$; (b) $x,\ y,\ z+1$; (c) $x,\ y,\ z-1$; (d) $-x+y+1,\ -x+2,\ z-1/3$; (e) $-x+y+1,\ -x+1,\ z-1/3$; (f) $-y+1,\ x-y,\ z+1/3$.

to intraligand π–π^* transition. Upon addition of CT-DNA to the complex solution, these intense intraligand absorption bands of the complex decrease (hypochromism, 8.4% at 225 nm and 7.5% at 271 nm), indicating an obvious binding of the complex with DNA. The intrinsic binding constant of the complex with CT-DNA was obtained using the following equation [27]: $[DNA]/(\varepsilon_a - \varepsilon_f) = [DNA]/(\varepsilon_b - \varepsilon_f) + 1/K_b(\varepsilon_b - \varepsilon_f)$, where [DNA] is the concentration of DNA in base pairs, ε_a is the apparent absorption coefficient, ε_f and ε_b represent the extinction coefficient for the free complex and the DNA-bound complex in the fully bound form, respectively. The intrinsic binding constant K_b, obtained from the ratio of the slope to the intercept in the plot of $[DNA]/(\varepsilon_a - \varepsilon_f)$ *versus* [DNA] (figure 3), is $9.50 \times 10^4\ M^{-1}$ L. The binding constant value indicates that the complex binds more strongly to DNA than $[Cr(salen)(H_2O_2)]^+$ and $[Cr(phen)_3]^{3+}$, whose binding constants are of

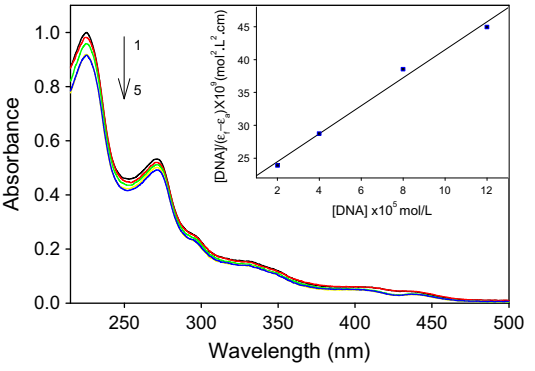

Figure 3. Absorption spectra of the complex in the absence and presence of the CT-DNA. [Complex] = 1.0×10^{-5} M L^{-1}, [DNA] = 0 (1), 2.0×10^{-5} (2), 4.0×10^{-5} (3), 8.0×10^{-5} (4) and 1.2×10^{-4} M L^{-1} (5), respectively. Arrows show the spectra changing upon increase in the CT-DNA concentration.

the order of 10^3–10^4 M^{-1} L [28, 29], but it binds more weakly to DNA than [Cr(DPPZ)$_2$Cl$_2$]$^+$ ($K_b = 1.8\times10^7$ M^{-1} L) [8]. In [CrCl(naph-gly)phen], the mixed ligands (naph-gly)phen possess a greater planar area than salen and phen, but a smaller planar area than DPPZ. The greater planar ligand can penetrate more deeply and stacks more strongly with the base pairs.

3.3.2. The fluorescence spectroscopy. Fluorescence spectroscopy has been used to investigate the interaction between the complex and DNA using EB as a probe [30]. EB emits intense fluorescence at 600 nm in the presence of DNA due to its strong intercalation between adjacent DNA base pairs. This enhanced fluorescence of EB-DNA can be quenched by the addition of a second molecule [31]. This property can be used to monitor the binding mode by the ability of a compound to prevent intercalation of EB from DNA. As shown in figure 4, the addition of the complex to DNA pretreated with EB causes an appreciable reduction in the fluorescence intensity, indicating that the chromium(III)

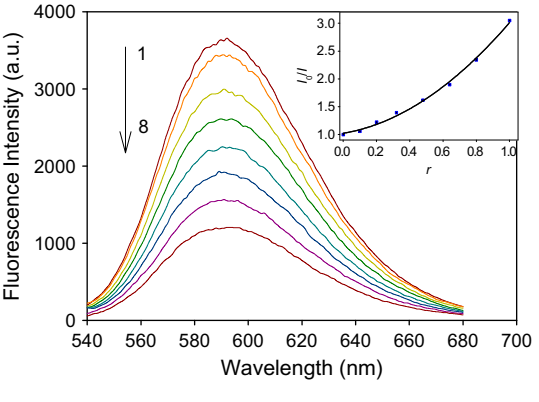

Figure 4. Emission spectra of EB-CT-DNA system in the absence (1) and presence of the complex (2–8), [EB] = 3.0×10^{-6} M L^{-1}, [DNA] = 2.5×10^{-5} M L^{-1}, r (the ratio of [Complex]/[DNA]) = 0, 0.10, 0.20, 0.32, 0.48, 0.64, 0.80, 1.00, respectively, λ_{ex} = 258 nm. The arrow shows increasing complex concentration. Inset: plot of I_0/I *vs*. r.

complex competes with EB to bind with DNA. The reduction of the emission intensity gives a measure of the DNA-binding propensity of the complex and stacking interaction between adjacent DNA base pairs [32]. The classical Stern–Volmer equation is used to quantitatively determine the magnitude of the binding strength of the complex with CT-DNA [33]. $I_0/I = 1 + K_{sq}r$, where I_0 and I represent the fluorescence intensities in the absence and presence of the chromium(III) complex, respectively, and r is the concentration ratio of the complex to DNA. K_{sq} is a linear Stern–Volmer quenching constant. As shown in the inset of figure 4, the Stern–Volmer plot indicated positive deviation from straight line. In general, positive deviation from linearity of Stern–Volmer plot occurs primarily when (a) combination of static and dynamic quenching takes place and/or (b) extent of quenching is large [34].

The apparent binding constant (K_{app}) was derived from the equation: K_{EB}[EB] = K_{app}[complex], where K_{EB} is 1.0×10^7 M^{-1} L and the concentration of EB is 3 μM L^{-1}; [complex] is the concentration of the complex causing 50% reduction in the emission intensity of EB [35]. The K_{app} value is 1.82×10^5 M^{-1} L for the complex, less than the binding constant of the classical intercalators and metallointercalators (10^7 M^{-1} L) [36], which suggests that the interaction of the complex with DNA is moderate intercalative mode.

3.3.3. CD spectra. To further investigate the nature of the binding mode between the complex and DNA, CD spectral experiment of CT-DNA with the complex was examined for its sensitivity to the mode of DNA interactions with small molecules [37]. The B-form conformation of DNA shows two CD bands in UV region, a positive band at 278 nm due to base stacking and a negative band at 246 nm due to polynucleotide helicity [33]. The changes in CD bands of DNA may indicate the interaction mode of DNA with small molecules. Groove binding and electrostatic interaction of DNA with small molecules show less or no perturbation on the base stacking and helicity bands, whereas intercalation can change the intensities of both of the two bands, thus stabilizing the right-handed B-conformation of DNA [38]. As shown in figure 5, upon increasing the concentration of the complex, both positive and the negative peaks of DNA showed obvious increase in intensity with slight

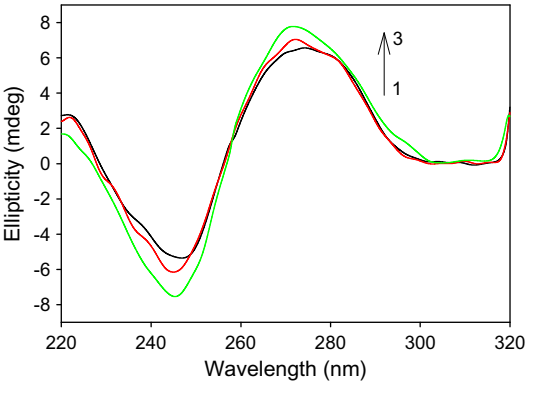

Figure 5. CD spectra of CT-DNA in the absence and presence of the complex. [DNA] = 1.0×10^{-4} M L^{-1}, [Complex] = 0 (1), 1.0×10^{-5} (2), 4.0×10^{-5} M L^{-1} (3), respectively. Arrows show the spectral changes upon increase in complex concentration.

blue shift of the maximum peak. The results showed that the mode of interaction between the complex and DNA should be intercalative [39].

3.4. *BSA-binding studies*

3.4.1. Fluorescence spectroscopy study. BSA has a strong fluorescence emission peak at 350 nm on excitation at 295 nm. BSA has two tryptophan residues that possess intrinsic fluorescence, Trp-134 in the first sub-domain IB of the albumin molecule and Trp-212 in sub-domain IIA. The fluorescence emission intensity depends mainly on the degree of exposure of the two tryptophans to polar solvents and also on the proximity of BSA to specific quenching groups [40, 41]. Fluorescence quenching can appear as a result of various intermolecular and intramolecular interactions, including molecular collisions (dynamic quenching), complex formation (static quenching), energy transfer, and/or conformational changes [42]. The different mechanisms of fluorescence quenching can be classified as either dynamic quenching or static quenching [43]. As shown in figure 6, upon addition of the complex, the emission intensity at 348 nm of BSA decreased, revealing the changes of the tryptophan environment of BSA [44]. Fluorescence quenching mechanism can be analyzed by the Stern–Volmer equation [45]: $I_0/I = 1 + K_q\tau_0[Q] = 1 + K_{sv}[Q]$, where I_0 and I represent the steady-state fluorescence intensities in the absence and presence of quencher, respectively, K_{sv} is the Stern–Volmer fluorescence quenching constant, [Q] is the concentration of quencher, τ_0 is the average bimolecular lifetime in the absence of quencher, and K_q is the bimolecular quenching rate constant. K_{sv} obtained from the plot of I_0/I vs [Q] (figure 6) was 8.0×10^4 M^{-1} L. The Stern–Volmer fluorescence quenching constant K_{sv} of the title complex is greater than that of [CrCl(sal-gly)phen] ($K_{sv} = 2.9 \times 10^4$ M^{-1} L) [11].

Generally speaking, for most protein molecules, τ_0 is about 10^{-8} s [46]. So $K_q = 8.0 \times 10^{12}$ L M^{-1} s^{-1} can be calculated by equation of $K_q = K_{sv}/\tau_0$. This K_q value is much greater than the maximum value (2.0×10^{10} M^{-1} L s^{-1}) for diffusion-controlled quenching process of biological macromolecules [41], indicating that the dominant quenching mechanism should be static rather than dynamic.

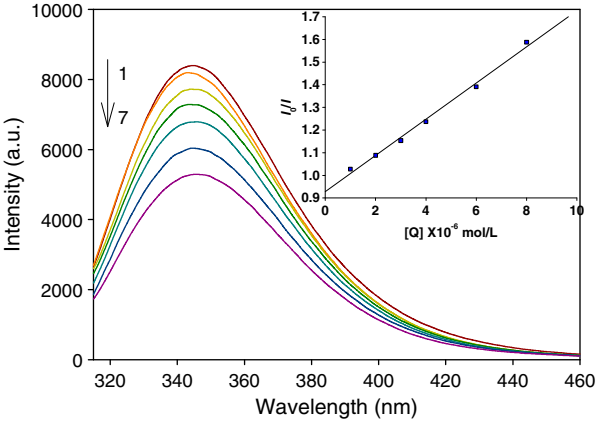

Figure 6. Fluorescence emission spectra of BSA in the absence and presence of the complex. [BSA] = 6.0×10^{-6} M L^{-1}, [Complex] = 0 (1), 1.0×10^{-6} (2), 2.0×10^{-6} (3), 3.0×10^{-6} (4), 4.0×10^{-6} (5) 6.0×10^{-6} (6), 8×10^{-6} M L^{-1} (7), respectively. λ_{ex} = 295 nm; both excitation and emission slits were 7 nm.

3.4.2. UV spectroscopic study. A simple method to explore the type of fluorescence quenching is UV–visible absorption spectroscopy. The static quenching refers to fluorophore–quencher complex formation in the ground state. In order to reconfirm the quenching mechanism, the absorption spectra of BSA in the absence and presence of the complex were determined. As shown in figure 7, the BSA spectrum has two main absorption peaks. The strong absorption at 208 nm is mainly due to the $\pi \rightarrow \pi^*$ transitions of the polypeptide backbone structure C=O groups [47]. The weak absorption at 278 nm could provide information about the three aromatic amino acids: tryptophan, tyrosine, and phenylalanine. The absorption intensity of BSA decreases with increasing complex concentration. The spectra of BSA in the absence and presence of this complex could not be superimposed, which also indicated that fluorescence quenching of BSA by this complex is mainly a static quenching procedure [48].

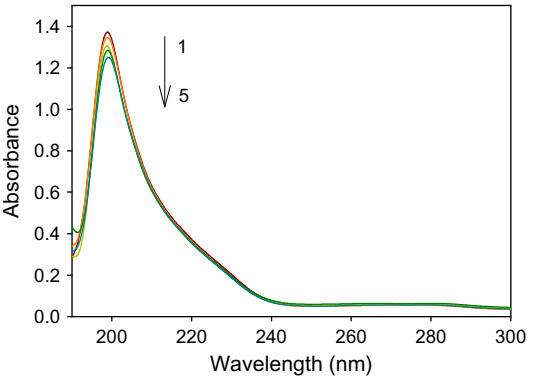

Figure 7. UV–visible spectra of BSA in the absence and presence of the complex at different concentrations. [BSA] = 5.0×10^{-7} M L^{-1}, [Complex] = 0 (1), 2.0×10^{-6} (2), 2.0×10^{-6} (3), 4.0×10^{-6} (4), 6.0×10^{-6} M L^{-1} (5).

3.4.3. CD study. CD spectroscopy is a powerful tool to investigate the secondary structure of a variety of biomolecular systems including proteins [49]. In order to verify the binding of the complex to BSA, CD spectral measurements were carried out. The results were expressed in terms of mean residue ellipticity (MRE) in deg·cm^2 dM^{-1} according to equation MRE = Observed CD (mdeg)/C_p nl × 10, where n is the number of amino acid residues (583 for BSA), C_p is the molar concentration of the protein, and l is the path length (0.1 cm).

BSA has a high percentage of α-helical structure, which shows a characteristic strong double minimum at 222 and 208 nm [50]. As shown in figure 8, upon addition of the complex, the intensity of double-humped peaks reduced, indicating that the extent of α-helix of BSA decreased. The α-helical content of BSA can be calculated from MRE values at 208 nm using the equation [51] α-helix(%) = [(–MRE_{208}–4000)/(33,000–4000)] × 100, where MRE_{208} is the observed MRE value at 208 nm, 33,000 is the MRE value of a pure α-helix at 208 nm, and 4000 is the MRE of the β-form and random coil conformation cross at 208 nm. When the molar ratio of the chromium(III) complex to BSA reached 2.0, the content of α-helix reduced from 54.92% in free BSA to 50.88%.

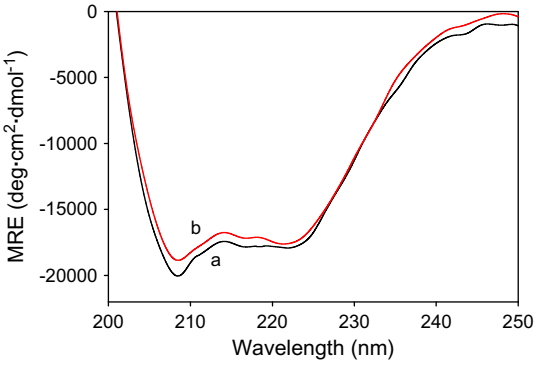

Figure 8. CD spectra of the BSA in the absence (a) and presence of the complex (b). The concentrations of complex and BSA were 2.0×10^{-6} M L^{-1} and 1.0×10^{-6} M L^{-1}, respectively.

4. Conclusion

A new Cr(III) complex, [CrCl(naph-gly)phen]·H_2O, has been synthesized and characterized by elemental analysis, IR spectra, and X-ray single-crystal diffraction. The DNA-binding and BSA-binding properties of the Cr(III) complex have been studied by UV–visible, fluorescence, and CD spectra. Results indicate that the Cr(III) complex binds to CT-DNA moderately in an intercalative mode and can quench the intrinsic fluorescence of BSA by static quenching, as well as inducing a conformational change with the loss of helical stability of the protein. This study may be useful for evaluating and understanding those factors that determine the DNA-binding mode and BSA-binding property of chromium(III) complexes.

Supplementary material

Detailed crystallographic data for the crystal structure analysis have been deposited with the Cambridge Crystallographic Data Center, CCDC No. 1012459. Copies of the information may be obtained free of charge from The Director, CCDC, 12 Union Road, Cambridge CB2 1EZ, UK (Fax: +44 1223 336033; Email: deposit@ccdc.cam.ac.uk or www.ccdc.cam.ac.uk).

Funding

This project was supported by the Undergraduate Scientific-Technological Innovation and Culture Innovation Foundation of Liaocheng University [grant number SF2013126] and the Natural Science Foundation of Shandong Province of China [grant number Y2004B02].

References

[1] P.M. Ronad, M.N. Noolvi, S. Sapkal, S. Dharbhamulla, V.S. Maddi. *Eur. J. Med. Chem.*, **45**, 85 (2010).
[2] S.K. Bharti, G. Nath, R. Tilak, S.K. Singh. *Eur. J. Med. Chem.*, **45**, 651 (2010).
[3] M.S. Nair, R.S. Joseyphus. *Spectrochim. Acta, Part A*, **70**, 749 (2008).

[4] V. Raparti, T. Chitre, K. Bothara, V. Kumar, S. Dangre, C. Khachane, S. Gore, B. Deshmane. *Eur. J. Med. Chem.*, **44**, 3954 (2009).
[5] K.R. Di Bona, S. Love, N.R. Rhodes, D. McAdory, S.H. Sinha, N. Kern, J. Kent, J. Strickland, A. Wilson, J. Beaird, J. Ramage, J.F. Rasco, J.B. Vincent. *J. Biol. Inorg. Chem.*, **16**, 381 (2011).
[6] D.M. Stearns, J.P. Wise Jr, S.R. Patierno, K.E. Wetterhahn. *FASEB J.*, **9**, 1643 (1995).
[7] R. Vijayalakshmi, M. Kanthimathi, V. Subramanian, B.U. Nair. *Biochem. Biophys. Res. Commun.*, **271**, 731 (2000).
[8] V.G. Vaidyanathan, B.U. Nair. *J. Inorg. Biochem.*, **95**, 334 (2003).
[9] V.G. Vaidyanathan, T. Weyhermuller, B.U. Nair, J. Subramanian. *J. Inorg. Biochem.*, **99**, 2248 (2005).
[10] J.R. Rao, R. Gayatri, R. Rajaram, B.U. Nair, T. Ramasami. *Biochim. Biophys. Acta*, **1472**, 595 (1999).
[11] H. Liu, L. Li, Q. Guo, J. Dong, J. Li. *Transition Met. Chem.*, **38**, 441 (2013).
[12] L.Z. Li, Z.H. Guo, Q.F. Zhang, T. Xu, D.Q. Wang. *Inorg. Chem. Commun.*, **13**, 1166 (2010).
[13] T. Xu, L.Z. Li, S.F. Zhou, G.Q. Guo, M.J. Niu. *J. Chem. Crystallogr.*, **35**, 263 (2005).
[14] L. Bian, L.Z. Li, Q.F. Zhang, H.L. Liu, D.Q. Wang. *Acta Chim. Sinica*, **69**, 1661 (2011).
[15] Q. Guo, L.Z. Li, J.F. Dong, H.Y. Liu, T. Xu, J.L. Li. *Spectrochim. Acta, Part A*, **106**, 155 (2013).
[16] L.Z. Li, Q. Guo, J.F. Dong, T. Xu, J.H. Li. *J. Photochem. Photobiol. B*, **125**, 56 (2013).
[17] J. Marmur. *J. Mol. Biol.*, **3**, 208 (1961).
[18] M.E. Reichman, S.A. Rice, C.A. Thomas, P. Doty. *J. Am. Chem. Soc.*, **76**, 3047 (1954).
[19] G.M. Sheldrick. *SADABS. Program for Scaling and Correction of Area Detector Data*, University of Göttingen, Göttingen (1997).
[20] G.M. Sheldrick. *SHELXS-97 Program for Crystal Structural Solution*, University of Göttingen, Göttingen (1997).
[21] G.M. Sheldrick. *SHELXL-97, Program for Crystal Structural Refinement*, University of Göttingen, Göttingen (1997).
[22] G.B. Deacon, R.J. Philips. *Coord. Chem. Rev.*, **23**, 227 (1980).
[23] R.K. Dubey, C.M. Mishra, A.N. Mishra. *Indian J Chem.*, **44A**, 1159 (2005).
[24] S.S. Bhat, A.A. Kumbhar, H. Heptullah, A.A. Khan, V.V. Gobre, S.P. Gejji, V.G. Puranik. *Inorg. Chem.*, **50**, 545 (2011).
[25] G. Micera, V.L. Pecoraro, E. Garribba. *Inorg. Chem.*, **48**, 5790 (2009).
[26] N. Butenko, A.I. Tomaz, O. Nouri, E. Escribano, V. Moreno, S. Gama, V. Ribeiro, J.P. Telo, J. Pesssoa, I. Cavaco. *J. Inorg. Biochem.*, **103**, 622 (2009).
[27] A. Wolfe, G.H. Shimer, T. Meehan. *Biochemistry*, **26**, 6392 (1987).
[28] R. Vijayalakshmi, M. Kanthimathi, V. Subramanian, B.U. Nair. *Biochim. Biophys. Acta*, **1475**, 157 (2000).
[29] R.T. Watson, N. Desai, J. Wildsmith, J.F. Wheeler, N.A.P. Kane-Maguire. *Inorg. Chem.*, **38**, 2683 (1999).
[30] J.B. Lepecq, C. Paoletti. *J. Mol. Biol.*, **27**, 87 (1967).
[31] B.C. Baugley, M. LeBret. *Biochemistry*, **23**, 937 (1984).
[32] A. Jayamani, V. Thamilarasan, N. Sengottuvelan, P. Manisankar, S.K. Kang, Y.-I. Kim, V. Ganesan. *Spectrochim. Acta, Part A*, **122**, 365 (2014).
[33] J.R. Lakowicz, G. Webber. *Biochemistry*, **12**, 4161 (1973).
[34] B. Chakraborty, S. Basu. *J. Lumin.*, **129**, 34 (2009).
[35] Y.Y. Kou, J.L. Tian, D.D. Li, W. Gu, X. Liu, S.P. Yan, D.Z. Liao, P. Cheng. *Dalton Trans.*, 2374 (2009).
[36] J. Qian, W. Gu, H. Liu, F.X. Gao, L. Feng, S.P. Yan, D.Z. Liao, P. Cheng. *Dalton Trans.*, 1060 (2007).
[37] V.I. Ivanov, L.E. Minchenkova, A.K. Schyolkina, A.I. Poletayer. *Biopolymers*, **12**, 89 (1973).
[38] A. Silvestri, G. Barone, G. Ruisi, D. Anselmo, S. Riela, V.T. Liveri. *J. Inorg. Biochem.*, **101**, 841 (2007).
[39] Z.F. Chen, Y.C. Liu, L.M. Liu, H.S. Wang, S.H. Qin, B.L. Wang, H.D. Bian, B. Yang, H.K. Fun, H.G. Liu, H. Liang, C. Orvig. *Dalton Trans.*, 262 (2009).
[40] T. Peters. *Adv. Protein Chem.*, **37**, 161 (1985).
[41] C.J. Halfman, T. Nishida. *Biochim. Biophys. Acta*, **243**, 294 (1971).
[42] R.S. Kumar, H. Bergh, G. Wagnières. *J. Solution Chem.*, **41**, 294 (2012).
[43] S. Ashoka, J. Seetharamappa, P.B. Kandagal, S.M.T. Shaikh. *J. Lumin.*, **121**, 179 (2006).
[44] N.S. Quiming, R.B. Vergel, M.G. Nicolas, J.A. Villanueva. *J. Health Sci.*, **51**, 8 (2005).
[45] J.R. Lakowicz. *Principles of Fluorescence Spectroscopy*, 2nd Edn, p. 237, Plenum Press, New York (1999).
[46] N. Zhou, Y.Z. Liang, P. Wang. *J. Photochem. Photobiol. A*, **185**, 271 (2007).
[47] X.C. Zhao, R.T. Liu, Z.X. Chi. *J. Phys. Chem. B*, **114**, 5625 (2010).
[48] Y.J. Hu, Y. Liu, J.B. Wang, X.H. Xiao, S.S. Qu. *J. Pharm. Biomed.*, **36**, 915 (2004).
[49] M. Sarkar, S.S. Paul, K.K. Mukherjea. *J. Lumin.*, **124**, 220 (2013).
[50] L. Wang, R.T. Liu, Z.X. Chi. *Spectrochim. Acta, Part A*, **76**, 155 (2010).
[51] Q. Xiao, S. Huang, Z.-D. Qi, B. Zhou, Z.-K. He, Y. Liu. *Biochim. Biophys. Acta – Proteins Proteomics*, **1784**, 1020 (2008).